Article

Reduced productivity and carbon drawdown of tropical forests from ground-level ozone exposure

Check for updates

Alexander W. Cheesman [1,2,12] ✉, Flossie Brown [2,3,12] ✉, Paulo Artaxo [4], Mst Nahid Farha [1,5], Gerd A. Folberth [6], Felicity J. Hayes [7], Viola H. A. Heinrich [2,8,9], Timothy C. Hill [2], Lina M. Mercado [2,10], Rebecca J. Oliver [10], Michael O' Sullivan [2], Johan Uddling [11], Lucas A. Cernusak [1] & Stephen Sitch [2]

Elevated ground-level ozone, a result of human activity, is known to reduce plant productivity, but its influence on tropical forests remains unclear. Here we estimate how increased ozone exposure has affected tropical-forest productivity and the global carbon cycle. We experimentally measure the ozone susceptibility of various tropical tree species, and then incorporate these data into a dynamic global vegetation model. We find that current anthropogenic-derived ozone results in a substantial decline in annual net primary productivity (NPP) across all tropical forests, with some areas being particularly impacted. For example, Asia sees losses of 10.9% (7.2–19.7%) NPP. We calculate that this productivity decline has resulted in a cumulative loss in carbon drawdown of 0.29 PgC per year since 2000, equating to ~17% of the tropical contemporary annual land carbon sink in the twenty-first century. We also find that areas of current and future forest restoration are disproportionately affected by elevated ozone. Future socioeconomic pathways that reduce ozone formation in the tropics will incur benefits to the global carbon budget by relieving the current ozone impacts seen across both intact forest and areas of forest restoration, which are critical terrestrial regions for mitigation of rising atmospheric carbon dioxide.

Elevated ground-level ozone (O_3) is a secondary air pollutant that has detrimental impacts on plant growth across the globe[1–3]. Increases in urbanization, industrialization and energy consumption throughout the last century have led to an increase in O_3 precursor emissions (for example, nitrogen oxides (NO_x) and volatile organic compounds (VOCs)) globally, while at the same time anthropogenic climate change has also altered atmospheric chemistry[4]. In combination, these factors have resulted in an increase in surface O_3 concentrations worldwide. Air-quality monitoring in the Northern Hemisphere has shown evidence for increases of between 30 and 70% in O_3 concentration across the twentieth century[5], and atmospheric chemistry models suggest that global mean O_3 concentrations have risen 11.7 ± 2.3 ppb between 1850 and 2014[6]. Since 1990, tighter emission controls in higher-income countries at the same time as rapid land-use land-cover change, biomass burning and population expansion across emerging economies have shifted the majority of anthropogenic precursor emissions from the temperate Northern Hemisphere to tropical and subtropical regions[7]. O_3 concentrations across the tropics are projected to rise further in the near future as a result of (1) increased precursor emissions under most socioeconomic pathways[6,8] and (2) changes to atmospheric chemistry in a warming world[4]. This elevated, and increasing, concentration of O_3 across the tropics will probably reduce tropical plant productivity

A full list of affiliations appears at the end of the paper. ✉e-mail: alexander.cheesman@gmail.com; florencealice.brown@env.ethz.ch

and growth[1], further exacerbating pressures on natural systems across the tropics[9], ecosystems critical to a stable global carbon cycle[10,11]. This impact of O_3 on the global carbon cycle (indirect climate forcing) as a result of elevated O_3, itself also a greenhouse gas, can be profound[1].

Due to a sparsity of tropical data, large-scale modelling studies have assumed that the susceptibility of tropical trees to O_3 is comparable to that seen in temperate or boreal species[1,12,13]. At the same time, being generally aseasonal and without stomatal exclusion of O_3 due to water limitation, the annual O_3 flux accumulation period in the humid tropics is greatly extended as compared to temperate ecosystems. These factors combine to mean that the magnitude of O_3 impacts on tropical forests are considered globally significant, with estimates of the reduction in carbon uptake in the Amazon basin due to elevated O_3 being of the same magnitude as the direct carbon losses associated with the often cited biomass burning in the 'arc of deforestation' (that is, 230 TgC yr^{-1})[13]. However, although O_3 pollution has been documented to impact trees across the tropics[14,15] and potential susceptibility has been examined through the identification of physical leaf injury[14,16–18] or in the determination of altered biochemical functioning[19,20], little work has been done to determine the impact of O_3 on the actual productivity of tropical-forest tree species, nor in using this observed susceptibility to more accurately predict the implications of O_3 damage in the tropics for global carbon cycling. Understanding the likely role anthropogenically derived O_3 has had in shaping productivity of tropical ecosystems is critical to improving our ability to understand how future changes in $[O_3]$ (a result of likely socioeconomic trajectories) will impact both intact forests and areas of potential forest restoration—a critical nature-based solution to address anthropogenic-driven climate change[21,22].

Here, we (1) experimentally identify the relative susceptibility to O_3 in a range of tropical tree species and (2) parameterize a dynamic global vegetation model (JULES), which, in combination with output from an up-to-date spatially explicit atmospheric chemistry model at an hourly resolution, was used to assess the regional and global impacts of changing atmospheric O_3 on the carbon cycle, and (3) consider how future $[O_3]$ may impact tropical forests and their restoration into the near future.

Susceptibility to O_3 in tropical tree species

Our experimental assessment of O_3 susceptibility in ten tropical-forest tree species was based on the response of total plant biomass to the estimated flux of O_3 into leaves (that is, accumulated phytotoxic O_3 dose above a threshold of 1 nmol m^{-2} s^{-1}, POD$_1$ mmol m^{-2}) of plants grown under a range of realistic daytime $[O_3]$ in open-top chambers under tropical conditions (Methods). We observed a large degree of variation in species-level O_3 susceptibility (Fig. 1 and Extended Data Fig. 1) irrespective of how stomatal flux to O_3 was estimated (Extended Data Table 1), with calculated POD$_1$ dose–response functions ranging from species showing only limited impacts of O_3 on whole plant biomass (for example *Darlingia darlingiana* (Proteaceae)) to those that were severely impacted (for example, *Theobroma cacao* (Malvaceae)).

To account for the observed variation in O_3 susceptibility between species and to allow for the extrapolation of our findings to the modelling of O_3 impacts across the hyperdiverse tropics, we considered the range of O_3 susceptibility we experimentally observed to be typical of tropical-forest species. Further work across phylogenetically distinct tropical biomes[23] would be needed to confirm this assumption; however, it allowed us to select three indicative susceptibilities based on the quartile distribution of O_3 susceptibility observed so far in tropical trees (Fig. 1). Specifically, these were low (the 25th percentile, −0.38% POD$_1^{-1}$), moderate (the 50th percentile, −0.50% POD$_1^{-1}$) and high (the 75th percentile, −0.95% POD$_1^{-1}$), representing a conservative interpretation of the observed distribution, and the fact that most tropical species will demonstrate an O_3 susceptibility among this range of scenarios (Extended Data Fig. 1). Our indicative levels include at their high end a level similar to that seen in deciduous larch (*Larix kaempferi*,
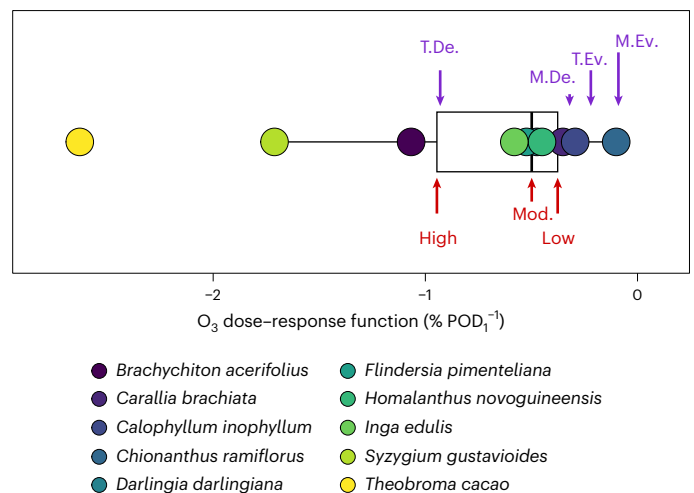

Fig. 1 | O_3 susceptibility of tropical tree species. The data represent the percent change in relative biomass per unit flux of O_3 into leaves above a threshold of 1 nmol m^{-2} s^{-1} (that is, POD$_1$) as determined in ten tree species. The 25th, 50th and 75th percentiles observed across our data (circles) were used in simulations of global tropical forests assuming one of three O_3 susceptibilities (low, moderate (mod.) and high), and are compared here to those used routinely when simulating temperate deciduous forests (T.De., typified by *Fagus sylvatica* and *Betula pendula*), temperate/boreal evergreen forests (T.Ev., typified by *Picea abies*), Mediterranean deciduous forests (M.De., typified by *Quercus robur*, *Quercus pyrenaica* and *Quercus faginea*) and Mediterranean evergreen forests (M.Ev., typified by *Quercus ilex*).

−0.99% POD$_1^{-1}$; ref. 24), and which is higher than both the O_3 'susceptible' temperate-deciduous birch and beech (T.De., −0.93% POD$_1^{-1}$) used in European-focused studies[25,26] and poplar (*Populus* cv., −0.75% POD$_1^{-1}$)[27]. Even as our moderate and low susceptibilities were found to be greater than that considered for either Mediterranean-deciduous forests (M.De −0.32% POD$_1^{-1}$)[25,28] or 'insensitive' temperate/boreal evergreen Norway spruce (*Picea abies*, T. Ev., −0.22% POD$_1^{-1}$)[25,26].

Regional impacts of O_3 on tropical-forest productivity

It has been estimated that tropical trees perform ~60% of the world's photosynthesis, capturing 72 PgC from the atmosphere every year[10]. However, by examining spatially explicit post-industrial changes in atmospheric $[O_3]$ (1900–2014; Fig. 2a and Extended Data Fig. 2), used to drive a dynamic global vegetation model (DGVM) parameterized to observed O_3 susceptibility of tropical trees (Extended Data Fig. 3), we show that anthropogenic-derived O_3 has probably reduced tropical-forest net primary productivity (that is, NPP during the period 2005–2014) by on average 5.1%, assuming a moderate O_3 susceptibility (this decline ranges from 3.4 to 9.6% assuming either low or high O_3 susceptibility; Table 1). Furthermore, this impact shows a great deal of geographic variation, from a decrease of 1.5% (1.0–2.8%) in Central Africa to 10.9% (7.2–19.7%) in Asian tropical forests (Table 1, Fig. 2 and Extended Data Fig. 4). This reflects both the recent rise in $[O_3]$ across South East Asia[29] and the fact that Central African tropical forests (for example, the Guinean forests of West Africa, Congo Basin and Eastern Afromontane) have probably been exposed to high $[O_3]$ since the pre-industrial era. As historic landscape management, which has included extensive biomass burning of savanna ecosystems[30], has meant that regions such as the Congo Basin have seen high seasonal O_3 exposure since before at least 1900[31,32] (Extended Data Fig. 2).

Cumulative impacts on carbon cycle

Our simulations suggest that changing $[O_3]$ across the twentieth and early twenty-first centuries (Extended Data Fig. 5) has led to a lost land
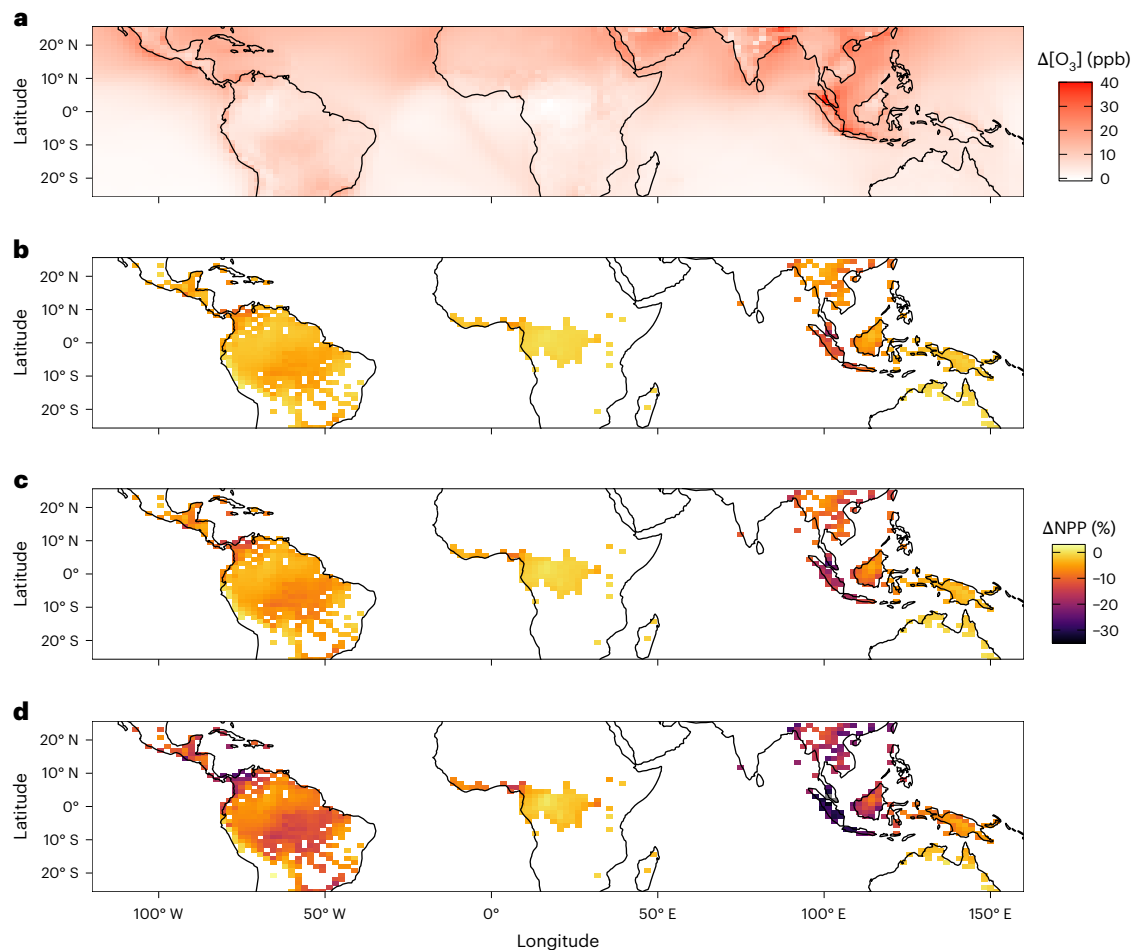
Fig. 2 | Changing ground-level O₃ and its impact on tropical-forest productivity. a–d, Pan-tropical change in annual ground-level [O₃] from 1900 to 2014 (**a**, data from UKESM1, CMIP6 historical simulation) as well as its current (2005–2014) impact on NPP of tropical forests, estimated using JULES and assuming one of three O₃ susceptibilities: low (**b**), moderate (**c**) and high (**d**). NPP data are only presented for grid cells in which tropical forests still represent >1% of total area. In the calculation of pan-tropical and regional impacts (Table 1), NPP is weighted by grid-cell area and the proportion of tropical forest remaining.

Table 1 | Impact of anthropogenic-derived O₃ on tropical-forest productivity

O₃ susceptibility	Pan-tropics	Central America[a]	South America	Africa[b]	Asia	Malay Archipelago	South Pacific[c]
High	−9.6	−12.5	−8.9	−2.8	−19.7	−18.1	−6.5
Moderate	−5.1	−6.4	−4.8	−1.5	−10.9	−10.1	−3.4
Low	−3.4	−4.1	−3.1	−1.0	−7.2	−6.7	−2.2

Data represent simulated decline in NPP (%) of tropical forests between 2005 and 2014 across geographical regions, and assuming one of three O₃ susceptibilities in tropical trees. [a]Central America, North America and West Indies. [b]Africa and Madagascar. [c]Melanesia, Micronesia and Australia.

sink of 21.1 PgC since 1900 (assuming moderate O₃ susceptibility), or 4.3 PgC and at a rate of 0.29 PgC yr⁻¹ since the year 2000 (or 0.24 and 0.47 PgC yr⁻¹, assuming low or high O₃ susceptibility, respectively). With losses in the twenty-first century representing ~17% of the contemporary tropical, and ~10% of the global natural land carbon sink over a similar period (that is, 1.71 ± 0.36 PgC yr⁻¹ and 3.07 ± 0.61 PgC yr⁻¹, respectively)[11], it is clear that the impact of air pollution on tropical forests has had, and continues to play, a substantial role in global carbon cycling.

Forest restoration at risk

Reforestation and afforestation of tropical ecosystems offer great potential to meet the global challenges of climate change, biodiversity decline and land degradation[33–35]. Understanding the rates and limitations of carbon sequestration into current and potential future restored landscapes will be critical to ensure accurate predictions

of future climate[21,36]. This must therefore include consideration of altered air quality[22]. Assuming a similar range in O₃ susceptibility across different tropical forest types, we find that areas of current secondary forest (that is, areas associated with previous deforestation and subsequent regrowth)[21] and potential forest restoration[37] (Extended Data Fig. 6) are both disproportionately impacted by declining air quality (Extended Data Fig. 7) as a result of their proximity to land-use land-cover change and/or urbanization[22]. As a result of this generally higher [O₃] the predicted %NPP losses found in areas of active secondary forest regrowth (0.3 million km²) are, on average, higher than that found in intact forests (13.2 million km²), with areas of potential forest restoration (4.0 million km²) demonstrating even greater vulnerability (Fig. 3 and Extended Data Fig. 8). As with intact tropical forests, the potential impact of O₃ on areas of current and future tropical-forest restoration shows a great deal of geographic variation. It is therefore
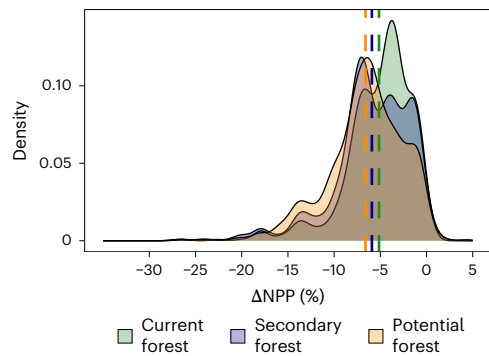
Fig. 3 | Impact of O$_3$ on productivity across different tropical forests.
Normalized distribution and area weighted mean (dashed lines) of predicted change in NPP across tropical forest types as a result of anthropogenically derived [O$_3$], assuming a moderate O$_3$ susceptibility. The figure represents the 10-year average (2005–2014) weighted by grid-cell area and fraction of existing tropical forests (average −5.1%), current secondary forests (average −5.9%) and areas of potential forest restoration (average −6.6%).

clear that accurate estimation of carbon sequestration potential must also account for the likely impacts of regional air quality.

Future impacts of air pollution

Atmospheric chemistry model projections from a range of future emission scenarios as part of Shared Socioeconomic Pathways (SSPs)[38] suggest a broad range in how [O$_3$] may change in the near future (2050, Extended Data Fig. 7) and by the end of century (2100)[8]. Standard scenarios agreed under ScenarioMIP[39] include those that result in increases (SSP3-7.0−Regional Rivalry with Climate Forcing from Greenhouse Gases, rising to 7.0 W m^{-2} by 2100; SSP5-8.5−Fossil-Fuelled Development, leading to forcing of 8.5 W m^{-2} by 2100), only a limited change (SSP2-4.5−Middle of the Road, with forcing rising to 4.5 W m^{-2}) and even a decrease (SSP1-2.6, Sustainability, which limits forcing to 2.6 W m^{-2}) in pan-tropical [O$_3$] (Extended Data Fig. 7). Yet, under all scenarios, anthropogenically derived O$_3$ will continue to impact the global carbon cycle and disproportionately impact regions of secondary forest considered critical for terrestrial mitigation of rising atmospheric CO$_2$ (Fig. 3 and Extended Data Fig. 7). It is also clear that the adoption of socioeconomic pathways that include greater environmental protection and the reduction in [O$_3$] through reduced precursor emissions (that is, SSP1-2.6) will incur additional benefits to the global carbon budget by relieving the current O$_3$ burden across both intact forest and areas of potential reforestation. The direct impacts of O$_3$ on tropical-forest productivity and thereby on climate warming need to be better represented in Earth System models, with a consideration of regional air quality included in carbon budgets and an assessment of efficacy in large-scale forest restoration efforts to combat global climate change.

Online content

Any methods, additional references, Nature Portfolio reporting summaries, source data, extended data, supplementary information, acknowledgements, peer review information; details of author contributions and competing interests; and statements of data and code availability are available at https://doi.org/10.1038/s41561-024-01530-1.

References

1. Sitch, S., Cox, P. M., Collins, W. J. & Huntingford, C. Indirect radiative forcing of climate change through ozone effects on the land-carbon sink. *Nature* **448**, 791–794 (2007).
2. Ainsworth, E. A., Yendrek, C. R., Sitch, S., Collins, W. J. & Emberson, L. D. The effects of tropospheric ozone on net primary productivity and implications for climate change. *Annu. Rev. Plant Biol.* **63**, 637–661 (2012).
3. Emberson, L. Effects of ozone on agriculture, forests and grasslands. *Philos. Trans. R. Soc. A* **378**, 20190327 (2020).
4. Brown, F. et al. The ozone-climate penalty over South America and Africa by 2100. *Atmos. Chem. Phys.* **22**, 12331–12352 (2022).
5. Tarasick, D. et al. Tropospheric Ozone Assessment Report: tropospheric ozone from 1877 to 2016, observed levels, trends and uncertainties. *Elem. Sci. Anth.* **7**, 39 (2019).
6. Turnock, S. T. et al. Historical and future changes in air pollutants from CMIP6 models. *Atmos. Chem. Phys.* **20**, 14547–14579 (2020).
7. Zhang, Y. Q. et al. Contributions of world regions to the global tropospheric ozone burden change from 1980 to 2010. *Geophys. Res. Lett.* **48**, e2020GL089184 (2021).
8. Griffiths, P. T. et al. Tropospheric ozone in CMIP6 simulations. *Atmos. Chem. Phys.* **21**, 4187–4218 (2021).
9. Malhi, Y., Gardner, T. A., Goldsmith, G. R., Silman, M. R. & Zelazowski, P. Tropical forests in the anthropocene. *Annu. Rev. Environ. Resour.* **39**, 125–159 (2014).
10. Mitchard, E. T. A. The tropical forest carbon cycle and climate change. *Nature* **559**, 527–534 (2018).
11. Friedlingstein, P. et al. Global carbon budget 2021. *Earth Syst. Sci. Data* **14**, 1917–2005 (2022).
12. Wang, Q. Y. et al. Evaluation of the impacts of ozone on the vegetation productivity of woodland and grassland ecosystems in China. *Ecol. Model.* **483**, 110426 (2023).
13. Pacifico, F. et al. Biomass burning related ozone damage on vegetation over the Amazon forest; a model sensitivity study. *Atmos. Chem. Phys.* **15**, 2791–2804 (2015).
14. Moura, B. B. et al. Ozone affects leaf physiology and causes injury to foliage of native tree species from the tropical Atlantic Forest of southern Brazil. *Sci. Total Environ.* **610**, 912–925 (2018).
15. Jamal, R. et al. Response of tropical trees to elevated ozone: a free air ozone enrichment study. *Environ. Monit. Assess.* **195**, 238 (2023).
16. Assis, P., Alonso, R., Meirelles, S. T. & Moraes, R. M. DO$_3$SE model applicability and O$_3$ flux performance compared to AOT40 for an O$_3$-sensitive tropical tree species (*Psidium guajava* L. 'Paluma'). *Environ. Sci. Pollut. Res.* **22**, 10873–10881 (2015).
17. Cassimiro, J. C. & Moraes, R. M. Responses of a tropical tree species to ozone: visible leaf injury, growth and lipid peroxidation. *Environ. Sci. Pollut. Res.* **23**, 8085–8090 (2016).
18. Fernandes, F. F. & Moura, B. B. Foliage visible injury in the tropical tree species, *Astronium graveolens* is strictly related to phytotoxic ozone dose (PODy). *Environ. Sci. Pollut. Res.* **28**, 41726–41735 (2021).
19. Schneider, G. F. et al. Current ambient concentrations of ozone in Panama modulate the leaf chemistry of the tropical tree *Ficus insipida*. *Chemosphere* **172**, 363–372 (2017).
20. da Silva Engela, M. R. C. et al. Metabolic and physiological alterations indicate that the tropical broadleaf tree *Eugenia uniflora* L. is sensitive to ozone. *Sci. Total Environ.* **769**, 145080 (2021).
21. Heinrich, V. H. A. et al. The carbon sink of secondary and degraded humid tropical forests. *Nature* **615**, 436–442 (2023).
22. Perring, M. P., Bullock, J. M., Alison, J., Holder, A. J. & Hayes, F. Out of sight, out of mind—but not out of scope: the need to consider ozone (O$_3$) in restoration science, policy and practice. *Restor. Ecol.* **30**, e13622 (2022).
23. Slik, J. W. F. et al. Phylogenetic classification of the world's tropical forests. *Proc. Natl Acad. Sci. USA* **115**, 1837–1842 (2018).
24. Hoshika, Y., Paoletti, E., Agathokleous, E., Sugai, T. & Koike, T. Developing ozone risk assessment for larch species. *Front. For. Glob. Change* **3**, 45 (2020).
25. CLRTAP et al. in *Manual on Methodologies and Criteria for Modelling and Mapping Critical Loads and Levels and Air Pollution Effects, Risks and Trends* Ch. 3 (UNECE, 2017).

26. Buker, P. et al. New flux based dose-response relationships for ozone for European forest tree species. *Environ. Pollut.* **206**, 163–174 (2015).

27. Hu, E. et al. Concentration- and flux-based ozone dose-response relationships for five poplar clones grown in North China. *Environ. Pollut.* **207**, 21–30 (2015).

28. Marzuoli, R. et al. Dose–response relationships for ozone effect on the growth of deciduous broadleaf oaks in Mediterranean environment. *Atmos. Environ.* **190**, 331–341 (2018).

29. Wang, H. L. et al. Global tropospheric ozone trends, attributions and radiative impacts in 1995-2017: an integrated analysis using aircraft (IAGOS) observations, ozonesonde and multi-decadal chemical model simulations. *Atmos. Chem. Phys.* **22**, 13753–13782 (2022).

30. van Marle, M. J. E. et al. Historic global biomass burning emissions for CMIP6 (BB4CMIP) based on merging satellite observations with proxies and fire models (1750–2015). *Geosci. Model. Dev.* **10**, 3329–3357 (2017).

31. Rowlinson, M. J. et al. Tropospheric ozone radiative forcing uncertainty due to pre-industrial fire and biogenic emissions. *Atmos. Chem. Phys.* **20**, 10937–10951 (2020).

32. Vieira, I. et al. Global reanalysis products cannot reproduce seasonal and diurnal cycles of tropospheric ozone in the Congo Basin. *Atmos. Environ.* **304**, 119773 (2023).

33. Girardin, C. A. J. et al. Nature-based solutions can help cool the planet—if we act now. *Nature* **593**, 191–194 (2021).

34. Riahi, K. et al. in *Climate Change 2022*: *Mitigation of Climate Change. Contribution of Working Group III to the Sixth Assessment Report of the Intergovernmental Panel on Climate Change* (eds Shukla, P. R. et al.) Ch. 3 (Cambridge Univ. Press, 2022).

35. Roe, S. et al. Land-based measures to mitigate climate change: potential and feasibility by country. *Glob. Change Biol.* **27**, 6025–6058 (2021).

36. Cook-Patton, S. C. et al. Mapping carbon accumulation potential from global natural forest regrowth. *Nature* **585**, 545–550 (2020).

37. Griscom, B. W. et al. Natural climate solutions. *Proc. Natl Acad. Sci. USA* **114**, 11645–11650 (2017).

38. Riahi, K. et al. The Shared Socioeconomic Pathways and their energy, land use and greenhouse gas emissions implications: an overview. *Global Environ. Change* **42**, 153–168 (2017).

39. O'Neill, B. C. et al. The Scenario Model Intercomparison Project (ScenarioMIP) for CMIP6. *Geosci. Model Dev.* **9**, 3461–3482 (2016).

¹College of Science & Engineering, James Cook University, Cairns, Queensland, Australia. ²Faculty of Environment, Science and Economy, University of Exeter, Exeter, UK. ³Institute for Atmospheric and Climate Science, ETH Zurich, Zurich, Switzerland. ⁴Institute of Physics, University of Sao Paulo, São Paulo, Brazil. ⁵Department of Chemistry, Rajshahi University of Engineering &Technology, Rajshahi, Bangladesh. ⁶UK Met Office Hadley Centre, Exeter, UK. ⁷UK Centre for Ecology & Hydrology, Environment Centre Wales, Bangor, UK. ⁸Remote Sensing and Geoinformatics, Helmholtz GFZ German Research Centre for Geoscience, Potsdam, Germany. ⁹School of Geographical Sciences, University of Bristol, Bristol, UK. ¹⁰UK Centre for Ecology & Hydrology, Wallingford, UK. ¹¹Department of Biological and Environmental Sciences, University of Gothenburg, Gothenburg, Sweden. ¹²These authors contributed equally: Alexander W. Cheesman, Flossie Brown. ✉e-mail: alexander.cheesman@gmail.com; florencealice.brown@env.ethz.ch

Methods

To assess the impact of changing O_3 exposure on tropical-forest systems, we experimentally determined the range of O_3 susceptibility observed in tropical tree species. Using this unique dataset, we then parameterized JULES, a DGVM. The validated model was subsequently used to explore the effects of anthropogenic-derived O_3 on current tropical-forest productivity, global carbon cycling and the potential implications for nature-based solutions to climate change in the future.

Experimental facility

All empirical work was conducted at the joint University of Exeter (UoE) and James Cook University (JCU) TropOz research facility (www.tropoz. org) located at the James Cook University's Environmental Research Complex (www.jcu.edu.au/environmental-research-complex) on the Nguma-bada campus in far-north Queensland, Australia[40,41]. The facility consists of nine independently controlled and monitored open-top chambers (OTCs), which allows the examination of plants grown under ambient CO_2 and nine different O_3 concentrations using a gradient experimental design[42]. The chambers (diameter 3.5 m, volume 22.2 m³) were ventilated with charcoal-filtered air (AireFlow-VC, Airpure Australia), into which O_3 generated on site (AirSep Onyx Plus O_2 generator and OZ-T4600 O_3 generator, Oxyzone International) was supplied between 8:00 and 17:00 to attain a range of nine different O_3 exposures, with typical mean chamber concentrations for each experiment ranging from 25 to 112 ppb during the hours of O_3 exposure. A single UV-absorption O_3 analyser (Model 205, 2B Technology) was used to continuously monitor [O_3] within the sample air being sequentially sourced from each chamber. A typical sampling sequence, accounting for solenoid switching and deadspace turnover, resulted in four readings (of 10-s instrument averages) per chamber every ~15 min. The chamber data were averaged and then interpolated via linear approximation to produce continuous dataset at a 5-min resolution for each chamber. Meteorological conditions including air temperature (T), relative humidity (RH) and photosynthetically active radiation (PAR) were recorded using a datalogger (Campbell Scientific) in the central OTC, with data averaged every 5 or 10 min. Exact experimental conditions (meteorology and O_3 exposure) for each OTC experiment are available in the associated data repository[43].

Plant material

Ten tropical tree species (Extended Data Table 1) from nine different families were selected to represent a broad range in successional stage and leaf morphological traits (that is, leaf mass per unit area (LMA) ranging from 58.1 to 142.5 g m⁻²). Species responses to O_3 were examined under a rolling experimental programme where different species were introduced to the chambers at different times and considered as independent of each other. All seedlings were sourced locally and planted when ~20 cm tall into either 20- or 60-l pots filled with locally sourced 'garden mix' topsoil mixed 3:1 with quincan (a local form of scoria) to improve drainage. Potted saplings were acclimatized to full sun before three or four replicate plants were transferred into each OTC, with typical O_3 fumigation for 9 h per day (from 8:00 to 17:00) and plants grown for between 61 and 191 (average = 150) days. Plants were irrigated daily using individual drip irrigation, and fertilized as required using a controlled-release fertilizer (Osmocote Native formula, ScottsMiracle-Gro).

At the end of the experiment, the plants were harvested for total biomass and separated into leaves, stems and roots to calculate biomass partitioning. Dry biomass was determined after oven-drying at 70 °C until a constant weight was achieved.

Calculating O_3 flux

To determine the accumulated phytotoxic O_3 dose (POD_y, mmol m⁻², above a threshold of y nmol O_3 m⁻² projected leaf area (PLA) s⁻¹) we used the deposition of O_3 for stomatal exchange (DO₃SE) model v. 3.1 (www.sei.org/tools/do3se-deposition-ozone-stomatal-exchange)[44] employing two methods of modelling dynamic stomatal conductance (g_s), specifically, a combined photosynthesis-stomatal conductance model assuming optimal stomatal behaviour[45,46] and an empirical-multiplicative g_s model.

The combined photosynthesis-stomatal conductance model was parameterized for each species using estimates of photosynthetic characteristics (for example, the maximum velocity of carboxylation, V_{cmax}, and the maximum rate of photosynthetic electron transport, J_{max}) and a stomatal response variable, g_1 (refs. 45,46; Extended Data Table 1) determined using a photosynthesis analyser (LI-6400XT, LiCOR Biosciences). Leaf-level gas exchange data were collected on the newest fully developed leaf of plants grown under the lowest [O_3] (control plants, typically $n = 4$) and consisted of both ACi curves (that is, plots of photosynthetic CO_2 assimilation versus CO_2 concentration inside the leaf) and survey measurements collected every 3 min for ~24 h per leaf using an inlet-buffer volume and with the LI-6400xt tracking ambient PAR and temperature. Average night-time conductance (that is, from 18:00 to 6:00) was taken as g_0, and daytime (6:00 to 18:00) gas exchange data were used to estimate leaf-level g_1 using the 'FitBB' function of the plantecophys package[47]. Fitting of ACi curves to determine V_{cmax} and J_{max} was carried out using 'plantecophys::fitaci' using updated default temperature response parameters (www.cran.r-project.org/web/packages/plantecophys/vignettes/new_T_responses.html).

We also carried out a parameterization of DO₃SE using an empirical-multiplicative g_s model[48,49]. In the weeks before harvesting, measurements of g_s were made on the youngest fully expanded mature leaf of all trees across the range in O_3 exposure using an SC-1 leaf porometer (Decagon Devices). Point measurements of g_s on both abaxial and adaxial leaf surfaces were collected over a range of time and weather conditions and coupled to the closest meteorological data as recorded by the experimental system. These values were used to parameterize the DO₃SE model (Extended Data Table 1) using the method described by in ref. 50, allowing for the calculation of POD_1 as per CLRTAP[25].

Ozone dose–response functions

Species-level O_3 dose–response functions were calculated using the linear decline in chamber-average relative biomass of each species against POD_1 determined using both a combined photosynthesis-stomatal conductance and empirical-multiplicative model of g_s. The relative biomass of each chamber was derived using the y intercept of a regression between average chamber total biomass and O_3 exposure (that is, the hypothetically maximum biomass at $POD_1 = 0$). It is important to note that this approach does not account for potential hormetic responses[51]; however, the slope coefficients of the linear dose–response function are still commonly used to calculate O_3 susceptibility[52]. Although the two methods used for calculating POD_1 generally agreed (Extended Data Fig. 1), we selected the observed distribution in O_3 susceptibility using the combined photosynthesis-stomatal conductance model to calibrate the JULES, given that the same model is employed within the DGVM itself.

Modelling framework

To examine the potential implications of O_3 on tropical forests, we used the Joint UK Land Environment Simulator (JULES, https://jules.jchmr.org) v. 5.6[53,54], a land surface model used to study the complex interaction of soil, water, vegetation and the atmosphere across the globe, used here with a spatial resolution of 1.25° latitude by 1.875° longitude. The modelling framework uses continuous and spatially explicit information about the environment and known changes in, for example, land use to allow us to model the response of vegetation to changing atmospheric composition, for example CO_2 (ref. 55), aerosols[56,57] and O_3 (ref. 58) and the influence of factors such as temperature[59] and drought[60].

The O_3 damage scheme employed in JULES v. 5.6 is the same as that implemented in refs. 1 and 61 (equations (1) to (3)), with updates

to plant functional types (PFTs) and their physiology as per refs. [62,63], and of photosynthetic and stomatal functional traits according to ref. [64]. The scheme works by modifying the net photosynthesis A_{net} of vegetation by an O_3 damage factor F (A_{mod}, equation (1)), with F defined by an O_3 sensitivity parameter α and the flux of O_3 into leaves above a threshold y (equation (2)). The decrease in photosynthesis results in a proportionate decline in NPP, with this model assuming (1) O_3 damage is instantaneous at the point of uptake and (2) there is a coordinated reduction in stomatal conductance g_s (equation (3)):

$$A_{mod} = A_{net} \times F \tag{1}$$

$$F = 1 - \alpha \times (\text{Flux } O_3 > y) \tag{2}$$

$$g_{mod} = g_s \times F \tag{3}$$

JULES routinely scales the flux of O_3 to the canopy by calculating it at each canopy layer and for shaded and sunlit leaves separately, whereas DO_3SE (used to determine O_3 susceptibilities) calculates for the uppermost sunlit leaves only. Therefore, to compare the dose–response function in JULES during calibration to those observed using DO_3SE, we used the O_3 flux to the top canopy layer sunlit leaves only, as in ref. [61].

Calibrating JULES to observed O_3 susceptibility of tropical trees

Given the broad range in O_3 susceptibility observed across the tropical tree species tested (Extended Data Fig. 1) and the lack of a clear link between O_3 susceptibility and basic leaf functional traits such as LMA, we calibrated the tropical broadleaf evergreen (BET-Tr) PFT to replicate one of three O_3 susceptibilities based on the range we observed (that is, low = -0.38% POD_1^{-1}, moderate = -0.50% POD_1^{-1} and high = -0.95% POD_1^{-1}). Calibration was achieved by iterative adjustment of the O_3 response factor of photosynthesis (α) after comparison of the annual NPP (years 2009–2011) with the observed dose–response functions (% biomass decline POD_1^{-1}) (Extended Data Fig. 3). It is important to note that this approach does assume that the impact of accumulated O_3 flux into plant leaves is a constant at the canopy scale. For additional modelled tropical PFTs, we chose to set the α of C_3 grasses to that observed in C_3 trees given the lack of comparable data, and for C_4 grasses that observed in *Saccharum spontaneum* cv. Mandalay[40] (that is, $\alpha = 0.04$ at a threshold of 2 nmol m^{-2} s^{-1}).

Simulation details

We ran pan-tropical simulations for the period from 1 January 1900 to 31 December 2014 (1900–2014) assuming a homogeneous O_3 susceptibility of tropical trees to one of the three levels identified (low, moderate and high) using a dynamic vegetation model[63,65], allowing the PFT fractional cover and leaf area index to change with the varying environmental conditions over the last century. Standard inputs across simulations included variation in [CO_2] and land-use land-cover change as used in the Global Carbon Budget 2020[66], with meteorology and forcing data from CRU-JRA v. 2.3[67]. To identify the impacts of anthropogenically derived O_3, we compared simulations with 'fixed' [O_3] representing the average seen between 1900 and 1910 to those with a 'transient' [O_3] (that is, 1900–2014). In both cases, [O_3] values were taken as an hourly input from UKESM1[68], part of a CMIP6 historical simulation[69], where all simulations included an initial 1,000-year model spin up (1900–1920 climatology cyclically repeated) with fixed [O_3].

Impacts of changing O_3 over the twentieth century

To examine the influence of changing [O_3] on current pan-tropical NPP, we examined the difference in modelled 10-year mean (2005–2014) NPPs of the BET-Tr PFT, in both fixed and transient [O_3] simulations. All BET-Tr performance data were weighted by current observed forest extent using the ESA CCI land-cover fractions (Extended Data Fig. 6) from 2015 translated into JULES PFTs as per ref. [70], as well as grid-cell extent. Broad geographic areas were assigned using Natural Earth (www.naturalearthdata.com).

In considering the cumulative impacts of changing [O_3] on tropical terrestrial carbon pools, we examined the time series of the total terrestrial pool size between static and transient [O_3] simulations, including the impacts of NPP decline, shifts in dynamic vegetation and changes in soil biogeochemistry. Rates of change were considered over the entire simulation (115 years, 1900–2014) as well as since 2000 (Extended Data Fig. 5).

Impacts of O_3 on nature-based solutions

To examine the potential impacts of O_3 susceptibility on nature-based solutions to climate change, we examined the impact of current (that is, 2014) air quality in regions of secondary forest regrowth[71] and potential forest restoration[37] assuming the same range in O_3 susceptibility across forest types. Original-resolution binary data were re-gridded to the resolution of the JULES model environment using the reproject function in the Google Earth engine (Extended Data Fig. 6). This allowed the calculation of each modelled grid cell covered by (1) existing forest, (2) secondary forest regrowth and (3) area of potential forest restoration.

In considering differences in the distribution of ΔNPP across forest types while addressing the challenge of examining differences in distributions across large datasets of different sizes (13.2 million km^2 of current forest, 0.3 million km^2 of current secondary forest and 4.0 million km^2 of potential forest), we coupled a systematic random-subsampling approach with the non-parametric two-tailed Kolmogorov–Smirnov (KS) test. Individual values for NPP decline were transformed into integers after multiplying by 100 (ΔNPP = -4.62 becomes -462 and so on) and the area-weighted data (that is, observed km^2 per unit ΔNPP) were expanded using the R function 'tidyr::uncount'. From these distributions we repeatedly drew a random sample of 1,000 observations from each forest type (current, secondary and potential) and applied the KS test to each pairwise comparison. As the KS test is influenced by sample size, it is more likely to produce an arbitrary significant result for large distributions, so we used this sampling approach to increase the chance of correctly detecting non-significant differences between groups. Reported distance (D statistics) and P values represent the mean values from 100 such iterative applications of the KS test to random subsets.

Data availability

The experimental data that support the findings of this study are available in the Dryad Data Repository at https://doi.org/10.5061/dryad.4b8gthtmz (ref. [43]).

Code availability

Code to make the figures found in this paper are available in the Dryad Data Repository at https://doi.org/10.5061/dryad.4b8gthtmz (ref. [43]).

References

40. Cheesman, A. W. et al. Impacts of ground-level ozone on sugarcane production. *Sci. Total Environ.* **904**, 166817 (2023).
41. Farha, M. N. et al. Examining ozone susceptibility in the genus *Musa* (bananas). *Funct. Plant Biol.* **50**, 1073–1085 (2023).
42. Kreyling, J. et al. To replicate, or not to replicate—that is the question: how to tackle nonlinear responses in ecological experiments. *Ecol. Lett.* **21**, 1629–1638 (2018).
43. Cheesman, A. W. et al. Data from: reduced productivity and carbon drawdown of tropical forests from ground-level ozone exposure. *Dryad* https://doi.org/10.5061/dryad.4b8gthtmz (2024).
44. Büker, P. et al. DO_3SE modelling of soil moisture to determine ozone flux to forest trees. *Atmos. Chem. Phys.* **12**, 5537–5562 (2012).

45. Medlyn, B. E. et al. Reconciling the optimal and empirical approaches to modelling stomatal conductance. *Glob. Change Biol.* **17**, 2134–2144 (2011).

46. Ball, J., Berry, J. & Woodrow, I. in *Progress in Photosynthesis Research* (ed. Biggins, J.) 221–224 (Springer, 1987).

47. Duursma, R. A. Plantecophys—an R package for analysing and modelling leaf gas exchange data. *PLoS ONE* **10**, e0143346 (2015).

48. Emberson, L. D., Ashmore, M. R., Cambridge, H. M., Simpson, D. & Tuovinen, J. P. Modelling stomatal ozone flux across Europe. *Environ. Pollut.* **109**, 403–413 (2000).

49. Jarvis, P. G. Interpretation of variations in leaf-water potential and stomatal conductance found in canopies in field. *Philos. Trans. R. Soc. Lond. B* **273**, 593–610 (1976).

50. Hayes, F., Harmens, H., Sharps, K. & Radbourne, A. Ozone dose-response relationships for tropical crops reveal potential threat to legume and wheat production, but not to millets. *Sci. Afr.* **9**, e00482 (2020).

51. Agathokleous, E. et al. Predicting the effect of ozone on vegetation via linear non-threshold (LNT), threshold and hormetic dose–response models. *Sci. Total Environ.* **649**, 61–74 (2019).

52. Pleijel, H., Danielsson, H. & Broberg, M. C. Benefits of the phytotoxic ozone dose (POD) index in dose–response functions for wheat yield loss. *Atmos. Environ.* **268**, 118797 (2022).

53. Clark, D. B. et al. The Joint UK Land Environment Simulator (JULES), model description—part 2: carbon fluxes and vegetation dynamics. *Geosci. Model Dev.* **4**, 701–722 (2011).

54. Best, M. J. et al. The Joint UK Land Environment Simulator (JULES), model description—part 1: energy and water fluxes. *Geosci. Model Dev.* **4**, 677–699 (2011).

55. Huntingford, C. et al. Simulated resilience of tropical rainforests to CO_2-induced climate change. *Nat. Geosci.* **6**, 268–273 (2013).

56. Rap, A. et al. Enhanced global primary production by biogenic aerosol via diffuse radiation fertilization. *Nat. Geosci.* **11**, 640–644 (2018).

57. Mercado, L. M. et al. Impact of changes in diffuse radiation on the global land carbon sink. *Nature* **458**, 1014–1017 (2009).

58. Leung, F. et al. CO_2 fertilization of crops offsets yield losses due to future surface ozone damage and climate change. *Environ. Res. Lett.* **17**, 074007 (2022).

59. Huntingford, C. et al. Implications of improved representations of plant respiration in a changing climate. *Nat. Commun.* **8**, 1602 (2017).

60. Harper, A. B. et al. Improvement of modeling plant responses to low soil moisture in JULESvn4.9 and evaluation against flux tower measurements. *Geosci. Model Dev.* **14**, 3269–3294 (2021).

61. Oliver, R. J. et al. Large but decreasing effect of ozone on the European carbon sink. *Biogeosci.* **15**, 4245–4269 (2018).

62. Harper, A. B. et al. Improved representation of plant functional types and physiology in the Joint UK Land Environment Simulator (JULES v4.2) using plant trait information. *Geosci. Model Dev.* **9**, 2415–2440 (2016).

63. Harper, A. B. et al. Vegetation distribution and terrestrial carbon cycle in a carbon cycle configuration of JULES4.6 with new plant functional types. *Geosci. Model Dev.* **11**, 2857–2873 (2018).

64. Oliver, R. J. et al. Improved representation of plant physiology in the JULES-vn5.6 land surface model: photosynthesis, stomatal conductance and thermal acclimation. *Geosci. Model Dev.* **15**, 5567–5592 (2022).

65. Cox, P. *Description of the TRIFFID Dynamic Global Vegetation Model*. Hadley Centre Technical Note 24 (Met Office, 2001).

66. Friedlingstein, P. et al. Global carbon budget 2020. *Earth Syst. Sci. Data* **12**, 3269–3340 (2020).

67. Harris, I. C. & University of East Anglia Climatic Research Unit. *CRU JRA v2.3: A Forcings Dataset of Gridded Land Surface Blend of Climatic Research Unit (CRU) and Japanese Reanalysis (JRA) Data; Jan. 1901–Dec. 2021* (NERC EDS Centre for Environmental Data Analysis, 2022).

68. Sellar, A. A. et al. UKESM1: description and evaluation of the U.K. Earth System Model. *J. Adv. Model. Earth Syst.* **11**, 4513–4558 (2019).

69. Eyring, V. et al. Overview of the Coupled Model Intercomparison Project Phase 6 (CMIP6) experimental design and organization. *Geosci. Model Dev.* **9**, 1937–1958 (2016).

70. Harper, K. L. et al. A 29-year time series of annual 300 m resolution plant-functional-type maps for climate models. *Earth Syst. Sci. Data* **15**, 1465–1499 (2023).

71. Vancutsem, C. et al. Long-term (1990–2019) monitoring of forest cover changes in the humid tropics. *Sci. Adv.* **7**, eabe1603 (2021).

Acknowledgements

Author contributions

A.W.C., P.A., G.A.F., F.J.H., T.C.H., L.M.M., J.U., L.A.C. and S.S. designed the concept and methodological approach used in this study. A.W.C., M.N.F. and L.A.C. carried out the empirical data collection with advice from F.J.H. and J.U. Modelling was led by F.B., with guidance from G.A.F. and S.S. and support in the form of code, data and advice from V.H.A.H., R.J.O. and M.O. A.W.C. and F.B. carried out the analysis and wrote the initial draft of the manuscript. All authors (A.W.C., F.B., P.A., M.N.F., G.A.F., F.J.H., V.H.A.H., T.C.H., L.M.M., R.J.O., M.O., J.U., L.A.C. and S.S.) discussed results, provided comments during the preparation of the manuscript and gave their approval for publication.

Competing interests

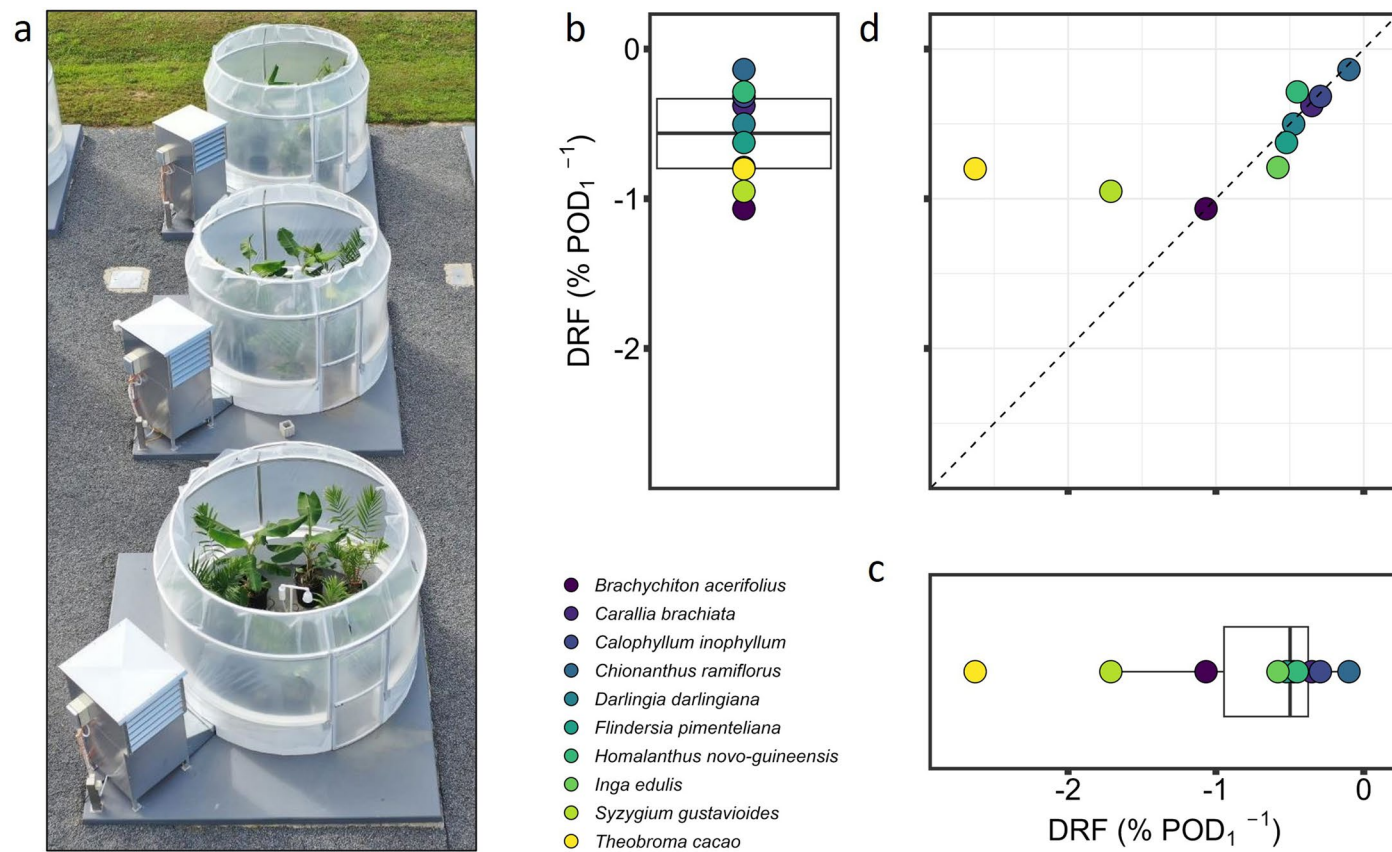The authors declare no competing interests.
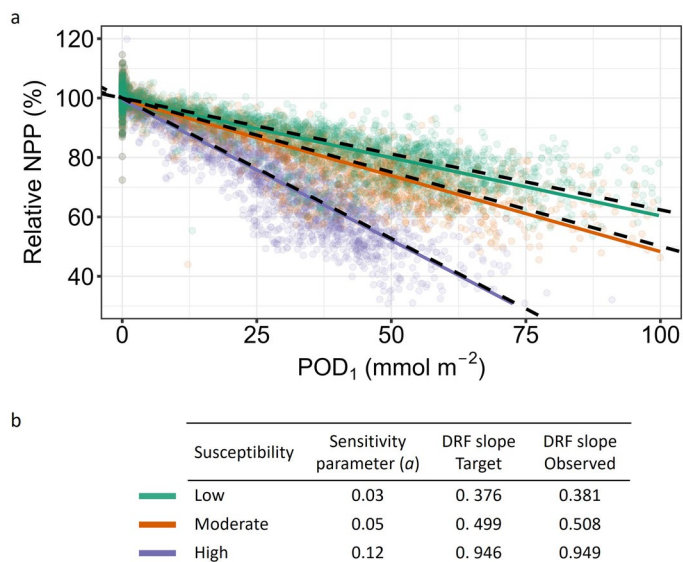
Additional information

Extended Data Fig. 1 | O3 susceptibility of tropical tree species. a–d, Change in relative biomass of tropical tree species (n = 10) grown in Open Top Chambers (**a**) under a range of [O_3] was used to calculate O_3 Dose Response Functions (DRF, % change in relative biomass POD_1^{-1}) determined through calculation of stomatal conductance using combined photosynthesis-stomatal conductance model (**b**), and empirical multiplicative g_s model (**c**). Boxplots show the range, median, interquartile-range of the data, while a comparison across species (**d**) shows general agreement between methods except for two species *Theobroma cacao* and *Syzygium gustavioides* due to stomatal behavior during leaf-level gas exchange data collection.
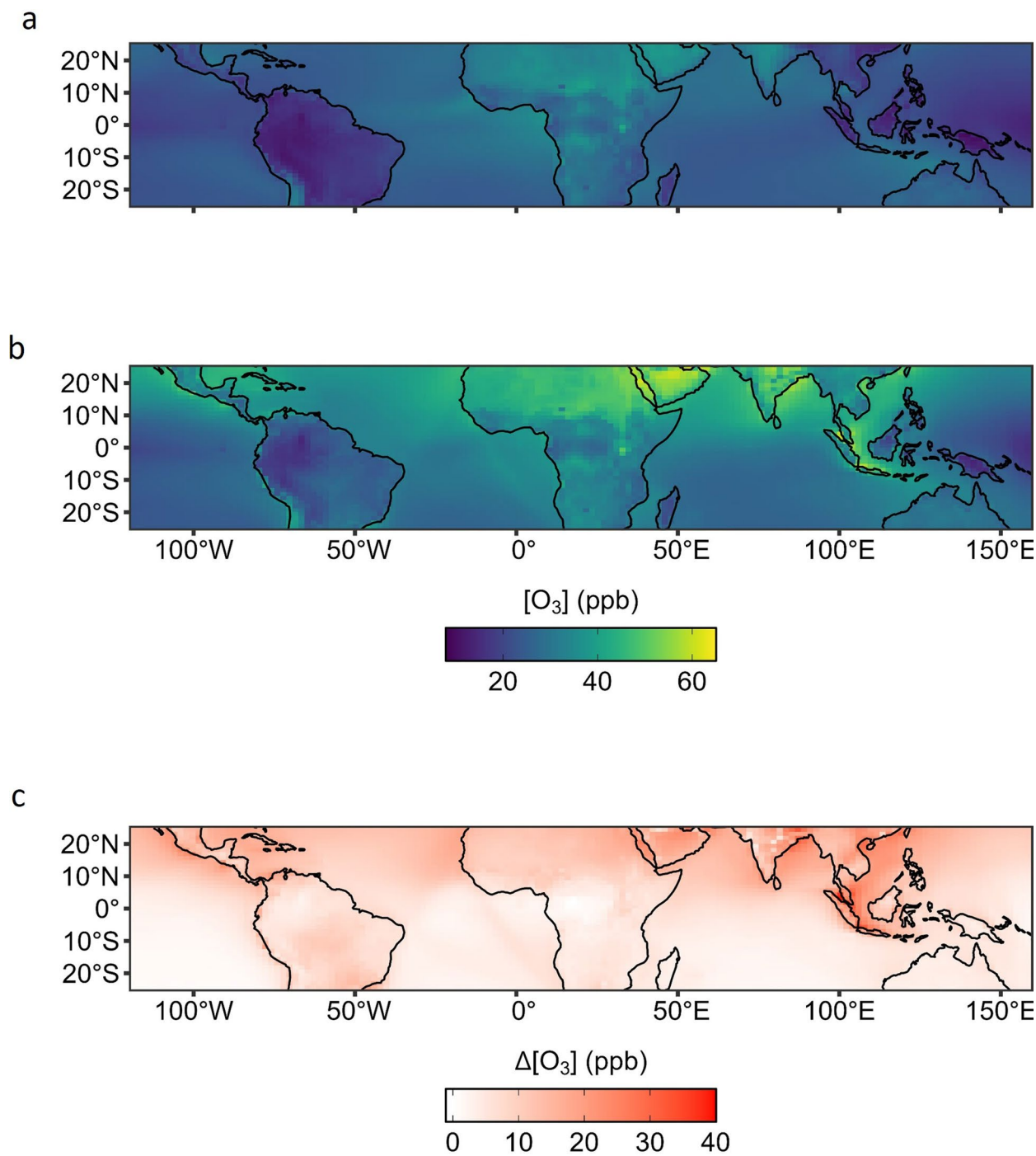
Extended Data Fig. 2 | Surface [O₃] from UKESM1 CMIP6 historical simulation used in JULES modelling at 1 h resolution. a–c, Data shown here represent 10-year annual mean during 1900 to 1909 (**a**), 2005 to 2014 (**b**), and the change in average mean [O₃] over the 20th century (**c**) as per Sellar et al.[68]. Note the largest absolute increases concurrent with tropical forests occurring over southeast Asia and the Amazonian Arc of Deforestation with little substantial change over the Congo basin as a result of high [O₃] in 1900 to 1909.
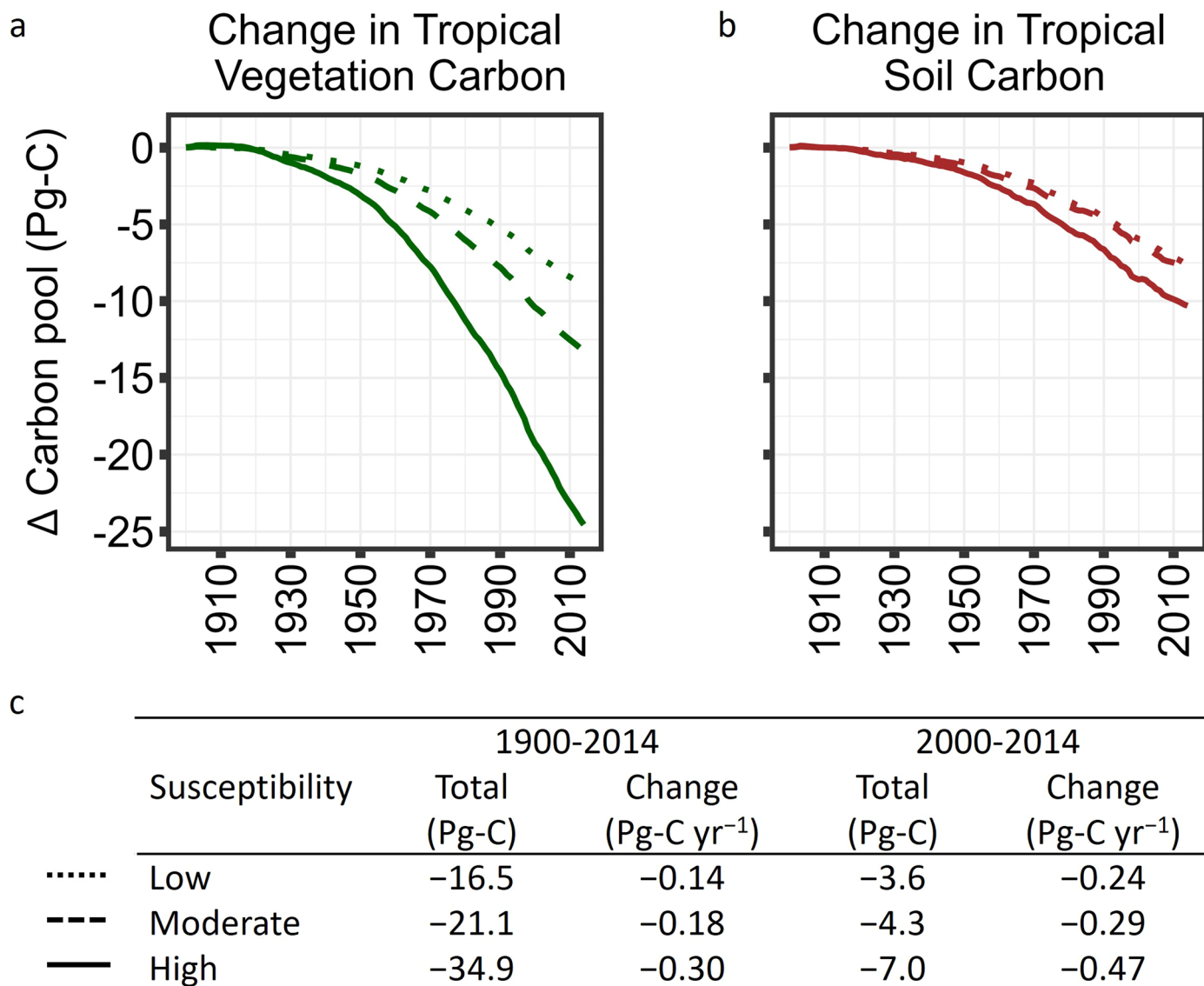
a

b

	Susceptibility	Sensitivity parameter (α)	DRF slope Target	DRF slope Observed
	Low	0.03	0. 376	0.381
	Moderate	0.05	0. 499	0.508
	High	0.12	0. 946	0.949

Extended Data Fig. 3 | Calibration of JULES O₃ response factor (α) for low, moderate and high O₃ susceptibility for the tropical broadleaf evergreen tree PFT (that is BET-Tr). a,b, The term α was calibrated to replicate three observed susceptibilities in biomass decline (that is low, moderate and high) by iterative adjustment. Figure demonstrates comparison of relative NPP across all gridcells with 100% forest cover in the years 2009, with target O₃ susceptibility (black dashed line) and performance of JULES using final α term used (coloured lines).
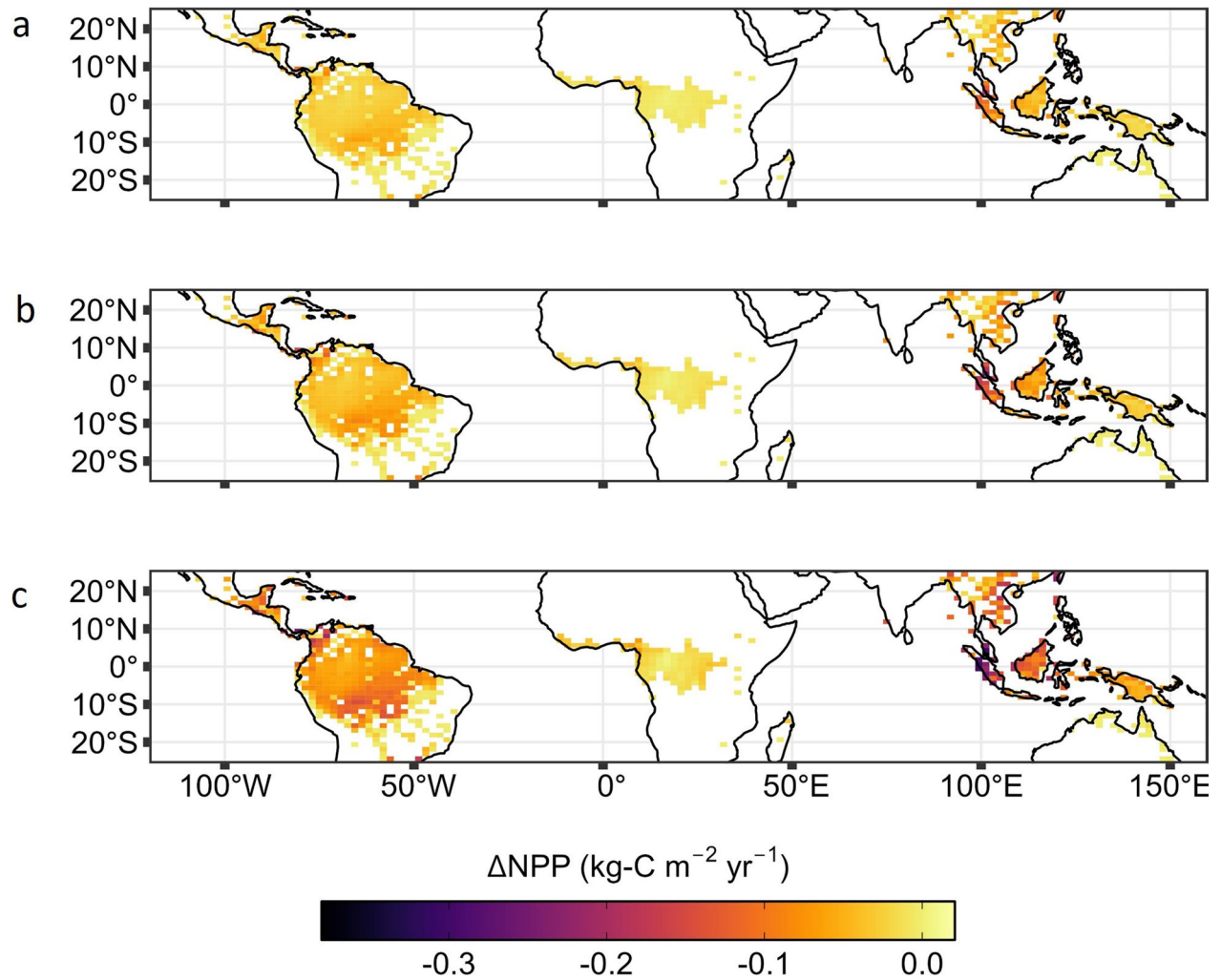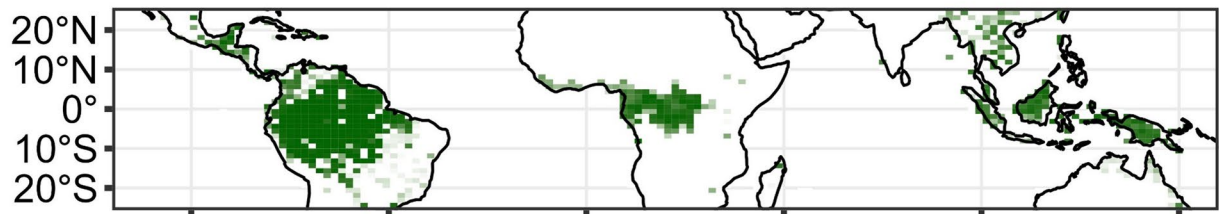
Extended Data Fig. 4 | Impact of anthropogenic-derived O$_3$ on tropical forest Net Primary Productivity. a–c, Data represents current (that is 2005 to 2014) decline in NPP (kg-C m^{-2} yr^{-1}) of tropical forests as estimated using JULES and assuming one of three O$_3$ susceptibilities, low (**a**), moderate (**b**), and high (**c**).

a

Change in Tropical Vegetation Carbon

b

Change in Tropical Soil Carbon

c

	Susceptibility	1900-2014		2000-2014	
		Total (Pg-C)	Change (Pg-C yr^{-1})	Total (Pg-C)	Change (Pg-C yr^{-1})
......	Low	−16.5	−0.14	−3.6	−0.24
---	Moderate	−21.1	−0.18	−4.3	−0.29
——	High	−34.9	−0.30	−7.0	−0.47

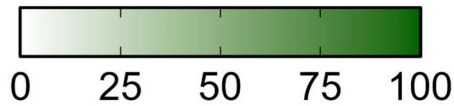**Extended Data Fig. 5 | Changes in tropical terrestrial carbon pools.** Specifically change in vegetation (**a**) soil (**b**) carbon over the 20th Century as a result of changing [O$_3$]. Simulated using an assumption of low (dotted), moderate (dashed) or high (solid) susceptibility to O$_3$ in tropical forest trees. Difference in total carbon pool held in the tropics (**c**) presented for the entire simulation (1900 to 2014) and for just the later-half of the 20th century (1960 to 2014) showing the increasing impact ground-level O$_3$ is having upon global carbon cycling.
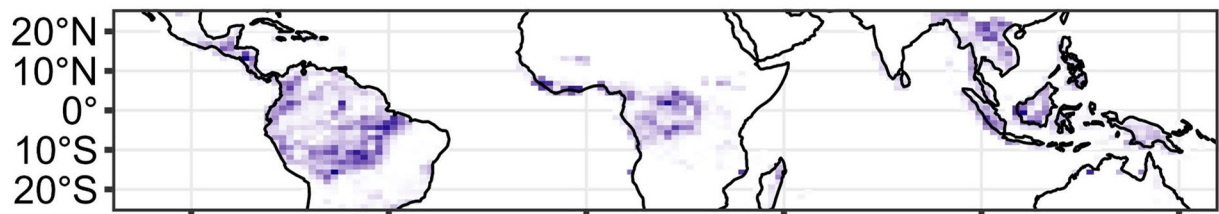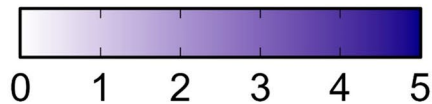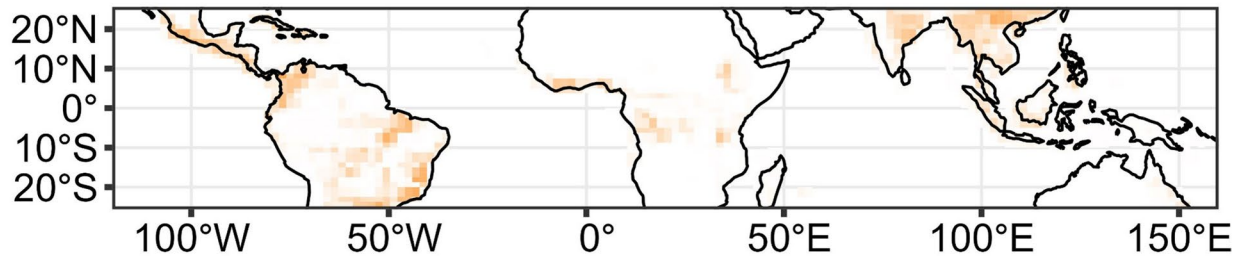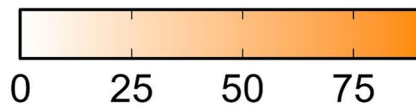
a

Current forest (%)

0   25   50   75   100

b

Secondary forest (%)

0   1   2   3   4   5

c

100°W   50°W   0°   50°E   100°E   150°E

Potential forest (%)

0   25   50   75

Extended Data Fig. 6 | Proportion of tropical forest types across grid cell areas within Dynamic Global Vegetation Modelling framework used. **a–c**, Areas of current forest based on the ESA CCI landcover fractions from 2015 translated into JULES PFTs as per Harper et al.[70] (**a**). Secondary forest representing areas that have been cleared and then revegetated after land abandonment or natural reforestation as per Vancutsem et al.[71] (**b**) and areas of potential forest restoration taken from Griscom et al.[37] resampled at appropriate resolution for JULES (**c**).
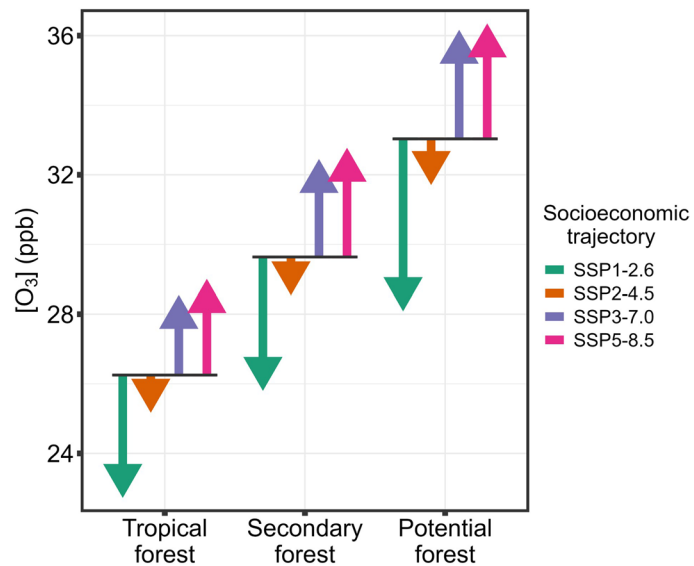
Extended Data Fig. 7 | Current and predicted change by the year 2050 in average annual [O₃] across tropical forests. Data represents UKESM1 CMIP6 (ref. 68) model results under different Shared Socioeconomic Pathways (SSPs)[38] across current tropical forest extent (that is, 13.2 million km²), current secondary forest (defined as areas that have been cleared, and then revegetated through land abandonment or active reforestation) (that is 0.3 million km²) and areas of potential forest restoration (that is 4.0 million km²).
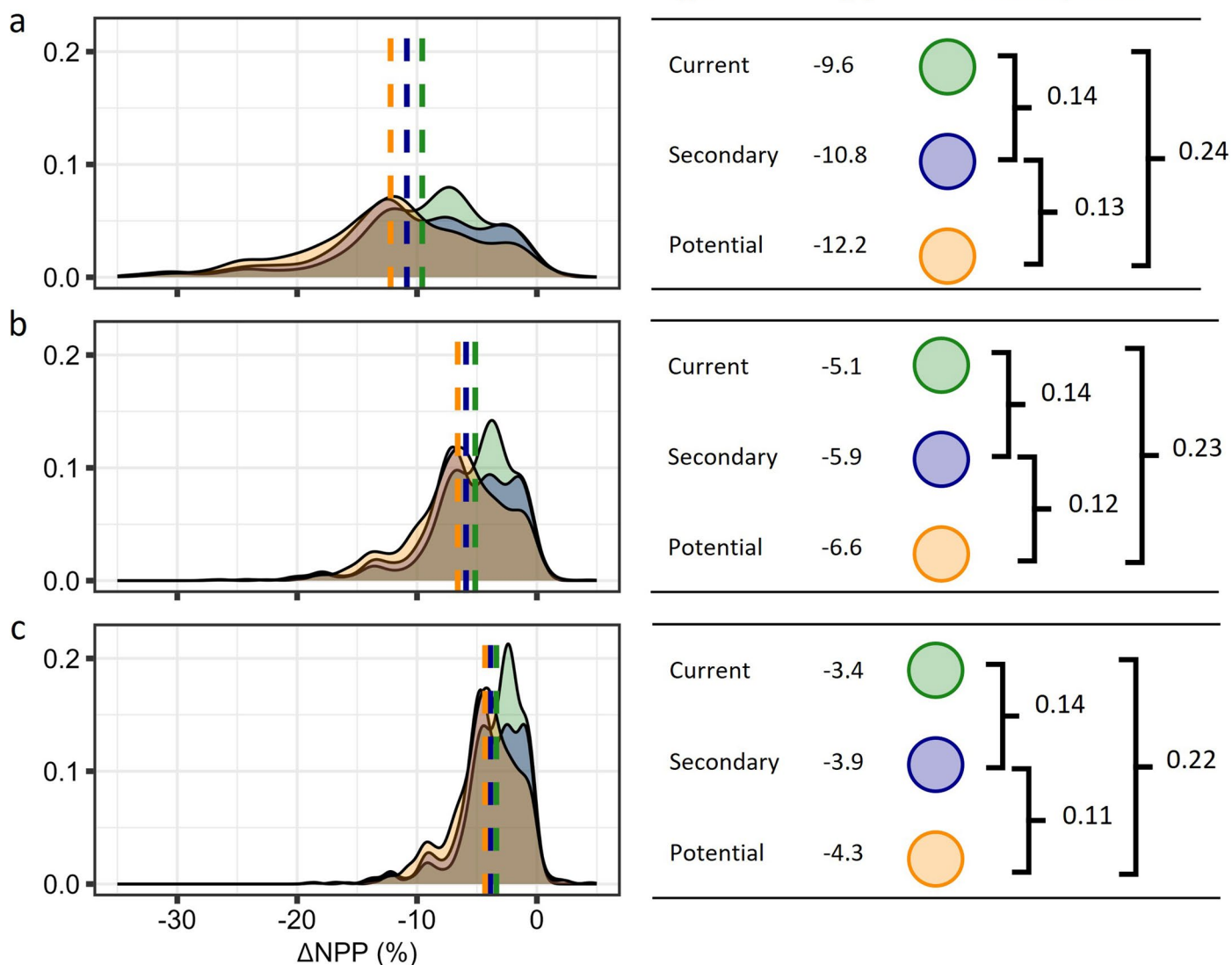
Extended Data Fig. 8 | Distribution of predicted change in modelled Net Primary Productivity (NPP) across tropical forests as a result of current [O₃], and assuming one of three O3 susceptibilities. a–**c**, Figures represent 10-year average (2005 to 2014) impact on the BET-Tr PFT weighted by gridcell area and fraction of gridcell representing current forests (13.2 million km²), current secondary forests (0.3 million km²), and areas of potential tropical forest restoration (4.0 million km²) and assuming high (**a**) moderate (**b**) or low (**c**) O₃ susceptibility in tropical trees. Dashed lines represent area weighted means of NPP decline. In testing for differences in distributions across forest types we applied the non-parametric two-tailed Kolmogorov-Smirnov Test using a systematic random-subsampling approach. Values reported for pairwise comparisons represent the average result of 100 iterations of KS test applied to a subset of 1000 observations of each forest type.

Extended Data Table 1 | Species-specific parameters used in DO$_3$SE model to calculate phytotoxic O$_3$ dose

	Units	Species[1]									
		Ba	Cb	Ci	Cr	Dd	Fp	Hn	Id	Sg	Tc
Photosynthetic model											
g_1	unitless	7.17	8.19	6.69	7.81	8.36	6.20	6.33	13.34	5.83	5.57
g_0	mmol H$_2$O m^{-2} s^{-1}	8.88	12.04	20.55	8.33	9.17	6.99	8.55	53.09	3.98	2.96
V_{cmax}	µmol CO$_2$ m^{-2} s^{-1}	51.0	45.0	58.6	48.6	32.9	41.6	66.6	47.1	34.8	27.3
J_{max}	µmol m^{-2} s^{-1}	138.6	137.9	127.9	122.5	108.5	71.8	192.2	137.7	108.4	63.5
Multiplicative model											
g_{O3}	mmol O$_3$ m^{-2} s^{-1}	135	166	184	126	154	79	296	279	149	167
f_{min}		0.07	0.07	0.11	0.07	0.06	0.09	0.03	0.19	0.03	0.02
T_{min}	°C	12	15	14	17	20	17	20	15	14	20
T_{max}	°C	45	49	45	47	45	45	46	45	45	50
T_{opt}	°C	27	32	30	32	32	30	33	30	30	35
VPD_{max}	kPa	1.9	2.5	2.8	2	2.3	2.5	2.5	2	2.5	2.5
VPD_{min}	kPa	4.5	5	4	5	3.6	5	7	3.8	3.7	6
PAR		0.016	0.006	0.005	0.007	0.008	0.01	0.004	0.01	0.013	0.008
Leaf-functional traits											
L_m	m	0.13	0.05	0.08	0.08	0.12	0.03	0.32	0.08	0.05	0.12
LMA	g m^{-2}	71.7	70.5	142.5	120.8	87.8	60.7	87.6	58.1	113.8	66.4

[1] Species codes: Ba = *Brachychiton acerifolius* (Malvaceae), Cb=*Carallia brachiata* (Rhizophoraceae), Ci=*Calophyllum inophyllum* (Calophyllaceae), Cr=*Chionanthus ramiflorus* (Oleaceae), Dd=*Darlingia darlingiana* (Proteaceae), Fp=*Flindersia pimenteliana* (Rutaceae), Hn=*Homalanthus novo-guineensis* (Euphorbiaceae), Ie=*Inga edulis* (Fabaceae), Sg=*Syzygium gustavioides* (Myrtaceae), Tc =*Theobroma cacao* (Malvaceae)

Species-specific parameters used in DO3SE model to calculate phytotoxic O3 dose. Data is from ten tropical tree species and includes basic leaf-level functional traits, including effective leaf width (Lm) and leaf mass per unit area (LMA).